WILEY | Hindawi

Research Article

Simulation Study of the Velocity Profile and Deflection Rate of Non-Newtonian Fluids in the Bend Part of the Pipe

Defeng Wang [iD],[1] Zhanbo Cheng,[2] Qingwen Shi,[3] Jinhai Zhao,[4] and Helmut Mischo [iD][1]

[1]*Institute of Mining and Special Civil Engineering, Technical University of Bergakademie Freiberg, Freiberg,*
  09599 Dresden, Germany
[2]*School of Engineering, University of Warwick, Coventry CV47AL, UK*
[3]*West Virginia University, Morgantown 26505, USA*
[4]*College of Energy and Mining Engineering, Shandong University of Science and Technology, Huangdao District,*
  266590 Qingdao, China

Correspondence should be addressed to Helmut Mischo; helmut.mischo@mabb.tu-freiberg.de

As resource extraction moves deeper underground, backfill mining has received a lot of attention from the industry as a very promising mining method that can provide a safe workplace for workers. However, the safe and efficient transport of fill slurry through pipelines still needs more exploration, especially in the bend section. In order to investigate the flow characteristics and velocity evolution of the slurry in the bend section of the pipe, a three-dimensional (3D) pipe model was developed using the computational fluid dynamics software Fluent, and nine sets of two-factor, three-level simulations were performed. Furthermore, a single-factor analysis was presented to investigate the effects of the two main influencing factors on the shifting of the maximum velocity of the slurry towards the distal side in the bend section, respectively. Then, the response surface analysis method was applied to the two-factor analysis of the maximum velocity shift and the weights of the two influencing factors were specified.

1. Introduction

Some of the world's biggest mining operations are currently at the stage of deep mining. For instance, the mining depth of coal resources has reached 1,500 m, the respective depth for the exploitation of geothermal resources has exceeded 3,000 m, and the mining depth of nonferrous metals has reached 4,350 m, while the exploitation of oil and gas resources has reached an astonishing depth of 7,500 m [1]. Based on forecasts made for the next ten to fifteen years, 50% of iron ore resources, 33% of nonferrous metal or mineral resources, and 53% of coal resources will be exploited at a mining depth of 1,000 m and below [2]. However, after the resource is mined out at such depths, significant geotechnical issues may increase. The vertical original rock stress caused by gravity and the tectonic stress generated by the addressed tectonic movement are basically exceeding the compressive level of the rock mass and the stress concentra-

tion level due to excavation, especially when large-scale mining activities take place. According to results of stress measurements in deep mining operations located in South Africa, at a depth ranging from 1 to 5 km, the ground stress can range from 50 to 135 MPa [3]. Other than that, according to surveys, in China alone, there are 1,600 coal gangue dumping fields, with a total volume of 4.5 billion tons, occupying a wide surface area [4].

The backfill mining method is a relatively new mining approach that can not only dispose of hazardous solid on the surface but also provide the operators underground a safe working space by supporting the adjacent rock mass or layers [5, 6]. In addition, a case study shows that the surface reclamation rate after filling and mining is up to 37.6% higher than that of other mining methods [7].

Therefore, with the further increase in environmental awareness, backfill mining has received unprecedented attention and many related practices were executed [8–10].
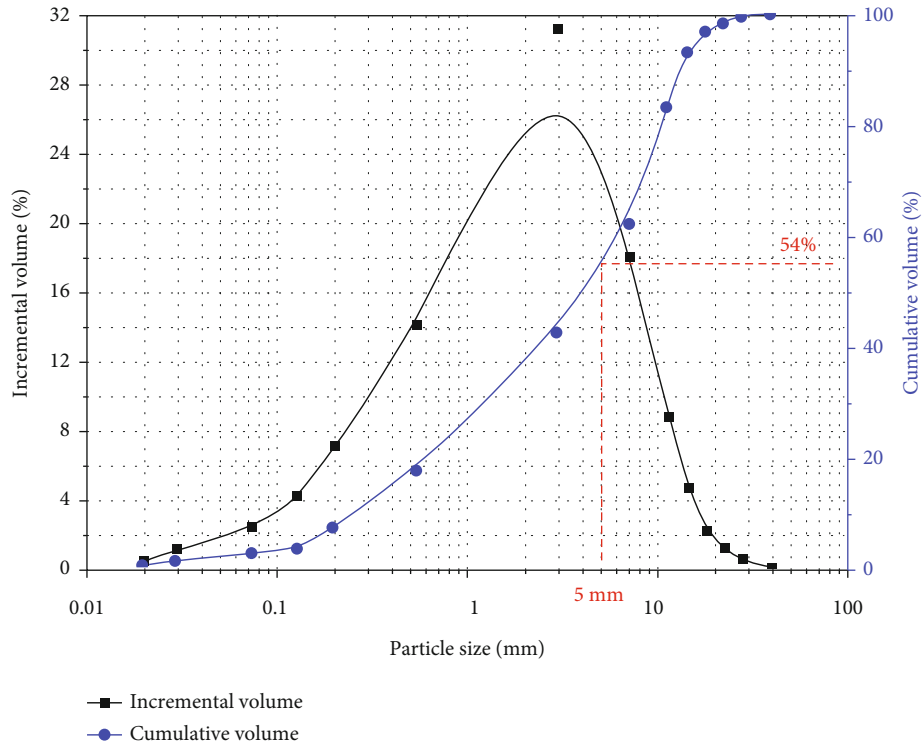
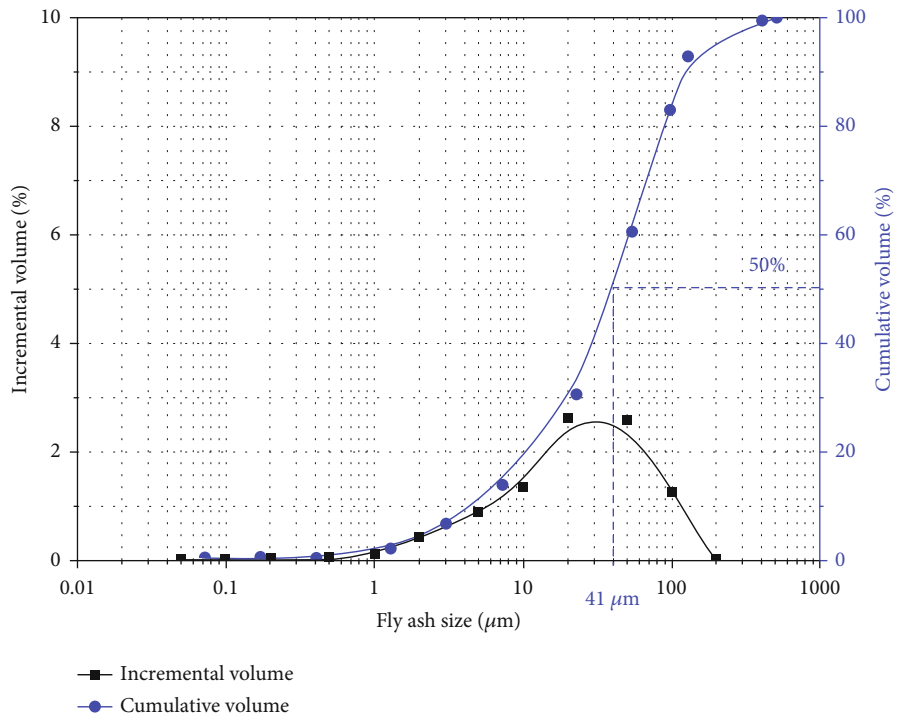FIGURE 1: Coal gangue particle size distribution.

FIGURE 2: Fly ash particle size distribution.

Furthermore, the continuous transport capacity of the pipeline system makes itself a superior transportation method that is being applied broadly [11, 12]. Accordingly, an intensive investigation was conducted in this research field [13].

For instance, Zhang et al. [14] analyzed the factors that affect the backfilling pipeline resistance of the tailing slurry, in order to accurately calculate the pressure loss. In another experimental and modeling study done by Qi et al. [15],

TABLE 1: Chemical composition of coal gangue and fly ash.

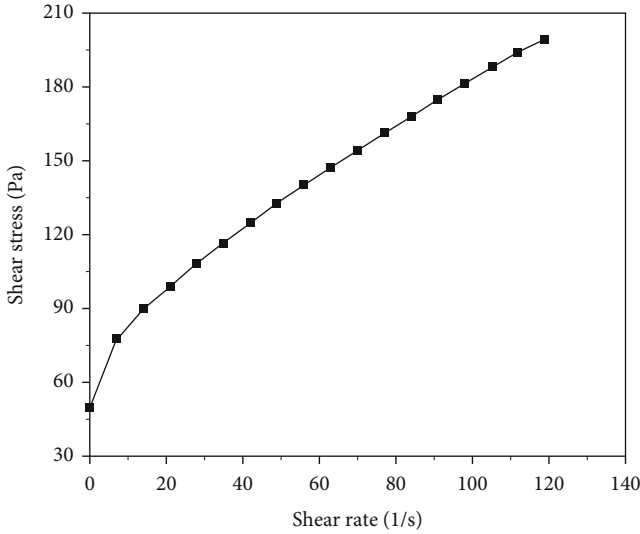| Classification	Composition	Loss	SiO_2	Fe_2O_3	Al_2O_3	CaO	MgO	TiO_2	Na_2O	K_2O
Gangue	Percentage (%)	17.8	51.92	3.87	19.03	1.0	1.18	0.75	0.54	1.47
Fly ash	Percentage (%)	10.33	43.84	27.40	4.01	12.13	1.09	—	—	—

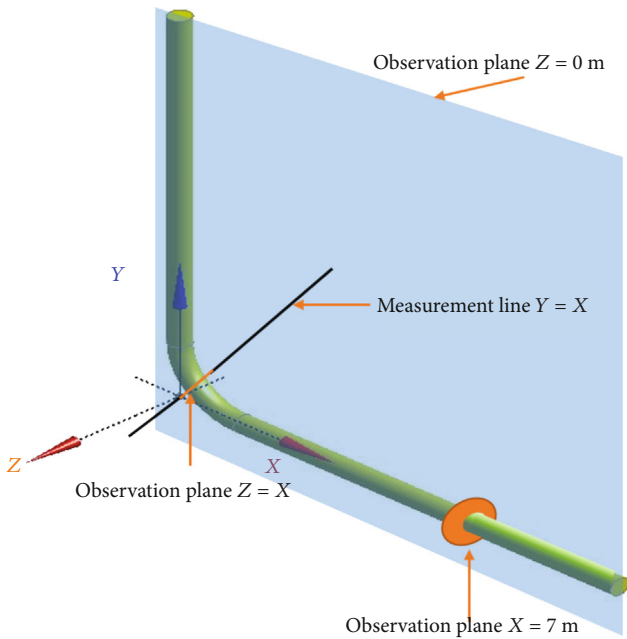FIGURE 3: Rheological features of slurry.

FIGURE 4: Geometry of the model.

the pressure evolution in pipe flow of cemented backfill is investigated. Liu et al. [16] compared experimental and simulation data in an effort to study the pipe flow characteristics of the cemented paste backfill slurry considering hydration effects.

In addition to the experimental study of the flow characteristics of fluids in pipes, many scholars adopted the numerical simulation method to reduce material and time costs [17–21]. In a research paper, Zhang et al. [22] predicted the erosion in a sharp bend geometry by applying a comprehensive CFD-based erosion prediction procedure, while Nuno and his colleagues [23] employed a computational fluid dynamics (CFD) model to analyze the laminar transients in pressurized pipes and proved that the strongest link between the wall shear stress and the axial component of the velocity occurs in the region close to the pipe wall as well as that the time shift between the wall shear stress and the local instantaneous flow acceleration increases significantly as time elapses.

The bend is an indispensable part of all pipeline transportation systems, and it is also the most easily worn or clogged place in the whole pipeline system. Although numerous experimental or simulation studies related to pipeline transportation are being carried out as described above, the velocity study of gangue fly ash high-concentration slurry in the bend part is still very limited. Thus, in this paper, computational fluid dynamics software was employed to reproduce the velocity characteristics of the slurry flowing through the bend part and to analyze how the influencing factors affect the offset of the velocity in the bend section of the pipe.

2. Material and Rheological Properties

The raw coal gangue used in this paper was collected from a coal mine located in Jining city, Shandong province, China. And after two stages of crushing, the processed coal gangue particle size is presented in Figure 1. From this figure, we can see that around 80% of the coal gangue particles are in sizes below 10 mm, and the particles smaller than 5 mm account for 54% of the total.

Fly ash (FA) is a byproduct produced during coal combustion in thermal power plants, with a large specific surface area and high adsorption activity. The particle size distribution of the fly ash being used in this paper is shown in Figure 2. And it is clear from this graph that the median particle diameter is 41 microns.

In addition to the size of the particles of the filling material which can have an influence on the properties of the slurry, the physical properties and chemical composition of the material are also factors that cannot be ignored. Nevertheless, the aforementioned properties of the filling material are not fixed; for example, the type of coal burned in a thermal power plant or even the manner and degree of burning of the coal can cause changes in the compounds of the fly ash particles. Hence, before preparing the filling material, the chemical composition of the particles needs to be specified in combination with an accurate measurement of the particle size distribution.
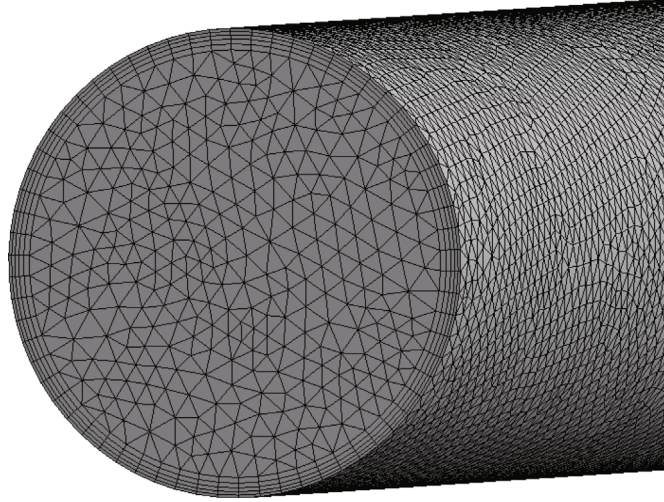
FIGURE 5: Mesh of the fluid domain.

TABLE 2: Model setting.

Diameter (m)	Velocity (m/s)	Concentration (%)
	2.0	
0.15	2.5	
	3.0	
	2.0	
0.18	2.5	76
	3.0	
	2.0	
0.21	2.5	
	3.0	

The physical and chemical properties of coal gangue and fly ash are shown in Table 1. The main phase of coal gangue is SiO_2, and the high content of SiO_2 indicates a decent compressive strength of the backfill mass. The content of the CaO in the fly ash accounts for 12.13%, and that defines the fly ash as a C type.

In the present study, fly ash and ordinary Portland cement (OPC) are mixed together as the binding agent in producing the backfill slurry, and the mixing ratio of FA and OPC by weight is 2 to 8, while the crushed coal gangue particles are used as aggregates.

After weighing the raw materials according to the planned proportion, the desired slurry with 76% solid concentration was mixed for 1 min at the speed of 100 r/min, then immediately transferred to rheological tests. The shear stress and shear rate relationships are demonstrated in Figure 3. However, the rheological curve shows a significant difference from that of a Newtonian flow; it is a nonlinear curve and needs critical stress to start the moving of the slurry flow. And according to some scholars' research, a suitable rheological model is the foundation that can achieve accurate prediction of flow characteristics [24–26]. Therefore, in this present paper, the Herschel-Bulkley model is adopted based on previous research studies [27–31].

3. Simulation Model

In order to reduplicate the flow characteristics of the CGFA slurry at the bend section of the pipeline, a 3D numerical model was developed as plotted in Figure 4. This model consists of three main parts (vertical section, bend section, and horizontal section), and the vertical section and the horizontal section were all set to be 10 m to ensure that a fully developed and stable slurry flow can be formed before or after passing through the bend section. The radius of the bend is 0.5 m. To facilitate the collection of fluid velocity information in the subsequent simulation experiments, a measurement line $Y = X$ was set up in the bend section. An observation plane at the measurement line position, as well as at the $X = 7$ m and $Z = 0$ m positions, was set up.

An appropriate discretization is a foundation for the subsequent simulation; therefore, it is vital to have a fine mesh for the targeted computational domain [32]. There are three main types of adaptive mesh generation approaches that are most commonly used in engineering applications: the triangulation method [33], the advancing front method [34], and the quadtree/octree method [35, 36]. Among these three types of methods, the triangulation method is automatic, robust, and easy to control mesh density. When the triangulation method is applied, the computation convergence can be ensured and the meshing results are optimized greatly. For this reason, triangular prisms are used in this paper. The independence of the mesh was proven since simulated pressures no longer exhibit nonnegligible differences when changing the mesh density. Moreover, considering the more complex flow conditions of the boundary layer fluid, five inflation layers were deployed to capture the boundary layer effects accurately (see Figure 5).

In the present paper, we focus on the effect of the slurry transport velocity and pipe diameter on the maximum offset ratio. For that purpose, three-level experiments on the two main factors are performed in the CFD simulation software, and the detailed simulation scheme is presented in Table 2.

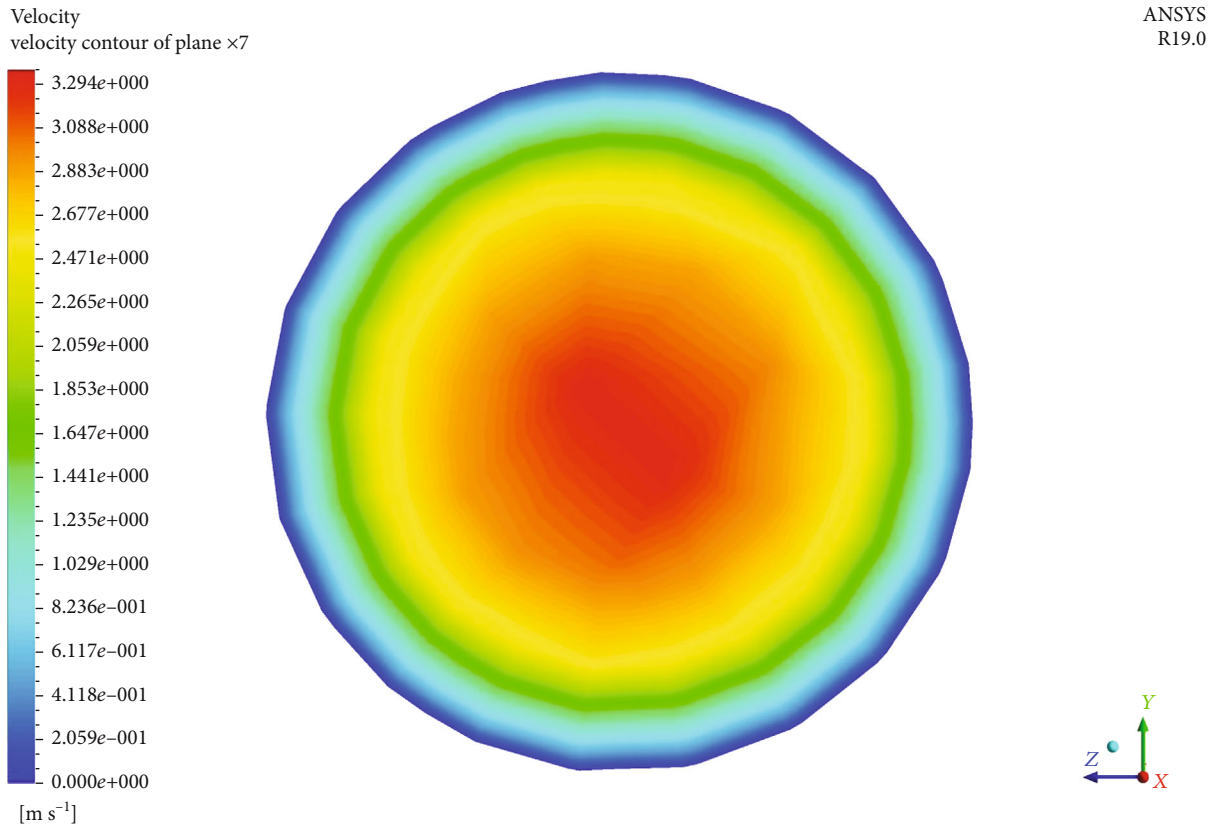Figure 6: Velocity contour of the observation plane $Z = 0$ m.

Figure 7: Velocity contour of the observation plane $X = 7$ m.
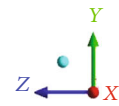
Velocity
velocity contour of plane ×05

- 3.294e+000
- 3.088e+000
- 2.883e+000
- 2.677e+000
- 2.471e+000
- 2.265e+000
- 2.059e+000
- 1.853e+000
- 1.647e+000
- 1.441e+000
- 1.235e+000
- 1.029e+000
- 8.236e−001
- 6.117e−001
- 4.118e−001
- 2.059e−001
- 0.000e+000

[m s^{-1}]
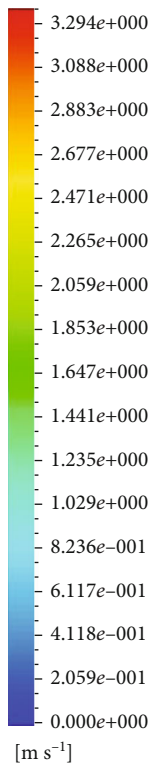
FIGURE 8: Velocity contour of the observation plane at the bend.

— V = 3 m/s, D = 0.21 m   - - - V = 2.5 m/s, D = 0.21 m
— V = 3 m/s, D = 0.18 m   — V = 2 m/s, D = 0.21 m
- - - V = 3 m/s, D = 0.15 m   - - - V = 2 m/s, D = 0.18 m
— V = 2.5 m/s, D = 0.15 m   — V = 2 m/s, D = 0.15 m
— V = 2.5 m/s, D = 0.18 m
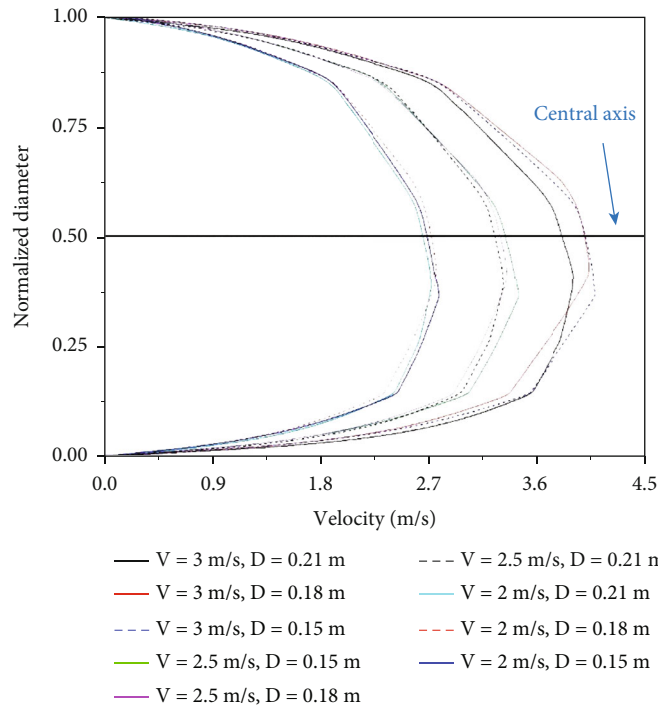
FIGURE 9: Velocity on the measurement line $X = Y$.

FIGURE 10: Offset ratio vs. velocity.

TABLE 3: Coded run scheme.

Run	Factor 1: diameter	Factor 2: velocity	Response: offset ratio
1	0.000	1.000	7.5
2	-1.000	0.000	13.8
3	0.000	-1.000	7.1
4	-1.000	-1.000	13.4
5	-1.000	-1.000	13.4
6	-1.000	1.000	13.4
7	1.000	-1.000	9.3
8	0.000	0.000	10
9	1.000	0.000	9.7
10	0.000	0.000	10
11	0.000	0.000	10
12	1.000	1.000	9.3
13	0.000	1.000	7.5
14	-1.000	-1.000	13.4
15	1.000	0.000	9.7
16	0.000	0.000	10

TABLE 4: Fit summary.

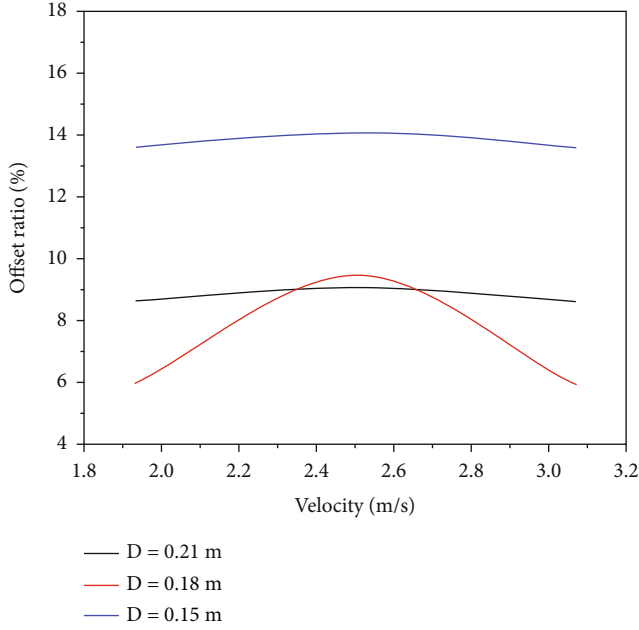| Source	Sequential p value	Adjusted R^2	Predicted R^2	
Linear	0.0070	0.4621	0.2643	
2FI	0.7769	0.4213	0.0054	
Quadratic	*<0.0001*	*0.9163*	*0.7622*	*Suggested*
Cubic	0.9600	0.8964	-2.7962	Aliased

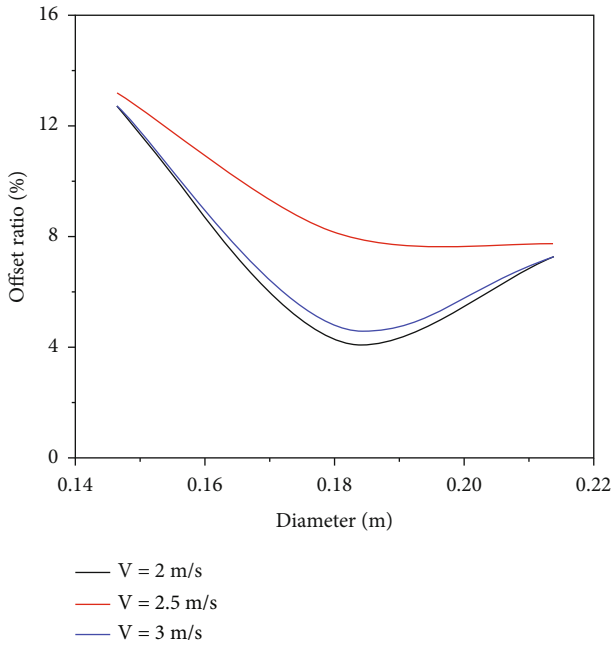

FIGURE 11: Offset ratio vs. diameter.

4. Results and Discussion

Following the setting of all parameters, the simulations are run, and hereinafter, the influence that the various pipe diameters and slurry flow velocities have on the velocity off-set is analyzed. The velocity contours on the observation planes aforementioned are plotted to show the velocity evolution when the slurry flows through the bend section of the pipe. Then, a single-factor analysis and a two-factor combined analysis are used to show how the two main influencing factors change the flow pattern of the slurry.

Since the distribution of velocity in the pipe and the tendency of deflection in the bend section are similar under different variables, in this paper, only the velocity contours are shown when the pipe diameter is 0.15 m and the slurry flow velocity is 2.5 m/s as demonstrated in Figures 6–8.

Figure 6 depicts a contour of velocities as the slurry flows through the pipe, from which we can clearly see the distribution of velocities and the large excursions that occur in the bend part of the pipe.

It can be seen that generally in the core section of the slurry flow, the velocity is larger than the margin layers close to the pipe wall. The reason behind this phenomenon is that, unlike in a Newtonian flow, the viscosity of the backfill slurry in the present study is relatively larger, and the slip velocity is positive near the pipe walls, whereas it is negative in the middle portion of the pipe cross-section. The same phenomenon was discussed in a study by Kumar et al. [37], in which they investigated the flow of highly concentrated iron ore slurry through a horizontal pipeline. Therefore, when the backfill slurry flows in a pipe, it forms a plug-like flow that has a special flow pattern with a distinguishing characteristic that the central section of the flow moves faster compared to its ambient flow section [38, 39]. And this velocity disparity is more intuitive and prominent in Figure 7.

TABLE 5: Coefficients in terms of coded factors.

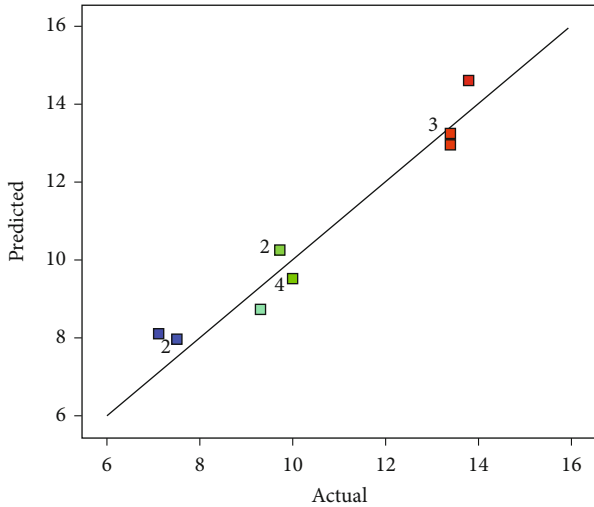| Factor	Coefficient estimate	df	Standard error	95% CI low	95% CI high	VIF
Intercept	9.52	1	0.2953	8.86	10.18	
A: diameter	-2.19	1	0.2387	-2.72	-1.66	1.15
B: velocity	-0.0584	1	0.2387	-0.5903	0.4736	1.15
AB	0.0707	1	0.2983	-0.5940	0.7354	1.16
A^2	2.92	1	0.3568	2.12	3.71	1.13
B^2	-1.49	1	0.3568	-2.29	-0.6997	1.13

FIGURE 12: Predicted offset ratio vs. actual offset ratio.

When the slurry flows through the elbow section of the pipeline, the slurry flow direction changes 90°, which denotes from vertical negative to horizontal. During this process, despite the fact that the slurry flow generally follows the original flow pattern attributed to the dominating role that the inertial force plays, the velocity profile changes dramatically. The largest velocity moves from the central region of the slurry flow to the pipe bottom as illustrated in Figure 8. The large difference between Figures 7 and 8 represents a huge change in velocity in the bend section, and an in-depth study of the change in velocity in the bend section is of great significance for the pipeline transport of the slurry.

Figure 9 shows the velocity profile reproduced from the velocity information collected on the measurement line. The diameters were normalized to facilitate the comparison of the velocity offset under different pipe diameters. From this figure, it can be seen that the positions where the highest velocities occur in the slurry are shifted towards the distal side of the bend which is consistent with the velocity contours presented above (see Figure 8). However, the slurry deflections at different combinations of the flow velocity and pipe diameter show a marked difference.

The offset ratio of the maximum velocity position (OROMVP) varies with the conveying velocity, and the changing tendency between different investigated velocity-diameter combinations shows vast variance (see Figure 10).

For instance, the OROMVP value of the slurry that flows in a pipe with a 0.15 m diameter is much larger than that of the other two counterparts. When the pipe diameter is 0.21 m or 0.15 m, the OROMVP reveals a gentle change with transport velocity, which implies that the maximum velocity of the slurry occurs at the same position when the slurry passes the bend section no matter what the transport velocity is. However, the OROMVP changes greatly with various flow velocities; when the pipe diameter is 0.18 m, it increases with the slurry conveying velocity until the conveying velocity reaches 2.5 m/s, and then the OROMVP decreases with the further increase of conveying speed.

Figure 11 demonstrates the effects of the pipe diameter on the OROMVP, and for all the three investigated groups, the largest OROMVP appears when the pipe diameter is 0.15 m. In terms of the slurry being transported at 2.5 m/s, the OROMVP decreases with the increasing conveying velocity although the speed of reduction becomes very slow when the pipe diameter exceeds 0.18 m. For the slurry that flows at 2 m/s, when the pipe diameter is in the interval of 0.15 m to 0.18 m, the OROMVP decreases with the rising pipe diameter, while when the pipe diameter is larger than 0.18 m, the OROMVP gradually increases with the increasing pipe diameter. And not only the tendency but also the values of the OROMVP of the slurry with a 3 m/s conveying velocity show a minor difference from that of the slurry with a 2 m/s conveying velocity.

A comparative analysis of Figures 10 and 11 shows that the 0.18 m diameter is special since, at this point, the OROMVP exhibits characteristics that clearly differ from other counterparts. Perhaps, designing the conveying system with a pipe diameter of about 0.18 meters can make the slurry velocity more stable when slurry flows through the bend section.

From the analysis in the previous section, it is clear that both the slurry transport velocity and the pipe diameter have a significant effect on the OROMVP, but it is not well explained how these two influences work together and what the respective weights of their contributions to the offset are. Therefore, the following parts will deal with this issue.

In order to determine the weights of the flow velocity and pipe diameter on OROMVP in the bend section, the response surface methodology (RSM) was adopted and run in a professional software program named Design-Expert (Stat-Ease Inc.). Response surface methodology [40] is a collection of mathematical and statistical techniques that can analyze all the dominant factors and how they influence
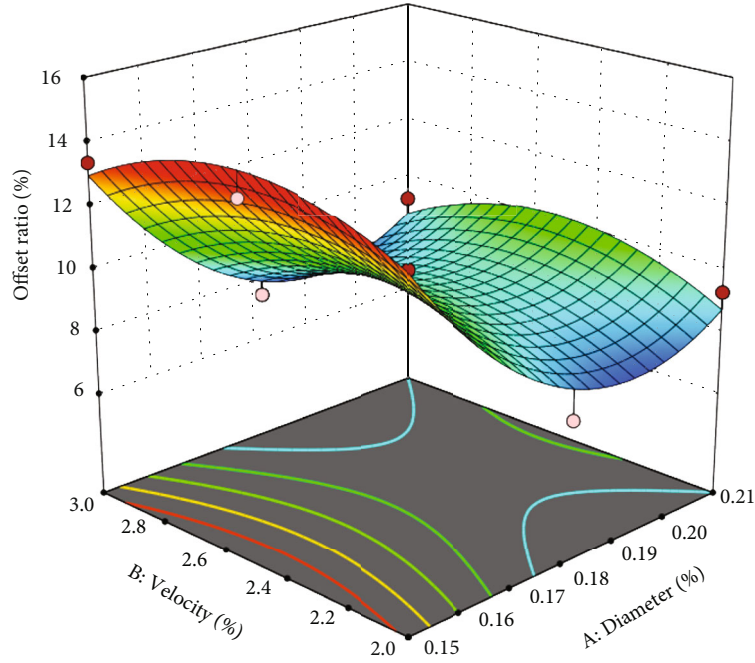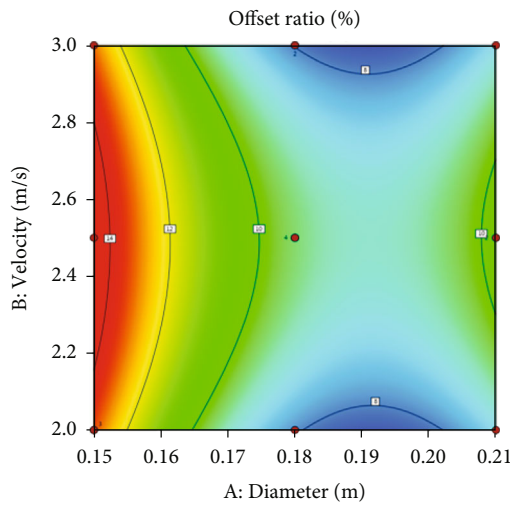
FIGURE 13: Response surface.

FIGURE 14: Two-dimensional projection of the response surface.

the dependent variables [41]. A central composite design with two independent variables (namely, the pipe diameter and slurry velocity) at three levels was performed by applying the Design-Expert 12.

The historical data RSM design and the response for this study can be found in Table 3. After 16 runs in total, the fit summary of different fitting models' accuracy and practicality is listed in Table 4, from which the most suitable model was automatically presented (denotes quadratic model in this present paper). And the adjusted R^2 and predicted R^2 indicate that the selected model has excellent accuracy.

The coefficient estimate represents the expected change in response per unit change in the factor value when all remaining factors are held constant while the intercept in an orthogonal design is the overall average response of all

the runs. The coefficients are adjustments around that average based on the factor settings, and the coefficients of all the independent variables are documented in Table 5. Based on the value of the estimated coefficient, the weights of each independent variable on the response variable were determined and the pipe diameter has a much more notable influence on the OROMVP than flow velocity. And the most influencing term is A^2, namely, the diameter-square.

The accuracy of the regression model was also ascertained since the experimental data and the model response are evenly distributed around the diagonal line in Figure 12. The actual value of the offset ratio represents the measured result for each experimental run while the predicted value is evaluated from the independent variables in the regression model.

In this paper, the three-dimensional plots and the two-dimensional contour depicted in Figures 13 and 14 were studied to investigate the behavior of the OROMVP from the interactions of the two operational variables.

The 3D plot, overall, appears to have a smooth saddle shape showing the effect of the combination of the flow velocity and pipe diameter on the OROMVP. It can be inferred from this figure that the effect of the pipe diameter in adjusting OROMVP at the bend section overwhelms that of the flow velocity as the OROMVP reflects a more pronounced change under the influence of varying the pipe diameter. The minimum OROMVP always occurs at a pipe diameter close to 0.18 m, when the pipe diameter varies from 0.21 m to 0.15 m, regardless of the flow velocity. Correspondingly, among all two-factor combinations of the flow velocity and pipe diameter, the OROMVP of the combination at a flow velocity of 2.5 m/s has been maintained as the largest. In the present paper, among all the investigated flow velocity and diameter combinations, the OROMVP of

the 0.15 m diameter and 2.5 m/s flow velocity group ranks the highest. When the pipe diameter is close to 0.19 m and the slurry transport velocity is more than 3 m/s or less than 2 m/s, the optimal OROMVP can be achieved. However, this conclusion was reached only considering the reduction of the OROMVP, and if more factors need to be included, such as filling efficiency or economics, a more comprehensive investigation is required.

5. Conclusion

Given the strong correlation between the velocity offset of the fluid flowing through the bend part and the damage to the bend, this paper focuses on the flow characteristics of the fluid in the bend part. In the present research, rheological parameters of the slurry were acquired by conducting a series of lab tests, and then the computational fluid dynamics simulation was operated to reproduce the fluid flow in the bend section, followed by an analysis of how the two influencing factors affect the OROMVP individually, and investigate how the two independent variables determine the OROMVP in the bend section by the response surface method. The following conclusions can be drawn:

(i) Although both the transport velocity and the pipe diameter have a significant effect on the OROMVP in the bend section, their weights differ significantly; in other words, the variation in the pipe diameter is more determinative

(ii) The critical conveying velocity for the slurry should be around 2.5 m/s since all the investigated samples show that conveying velocities above or below 2.5 m/s lead to a decrease in the OROMVP in the bend section. Therefore, in order to clarify the effect of conveying velocity on the OROMVP, further studies for the extended velocity range need to be conducted

(iii) The 3D response surface demonstrates the good performance of the 0.19 m diameter pipe in reducing the OROMVP of the slurry passing through the bend section. Therefore, under the premise of satisfying the mine filling efficiency, it is recommended to adopt 0.19 m pipes for slurry transportation to reduce damage such as abrasion of the pipe at the bend part

Data Availability

The data used to support the findings of this study are available from the first author upon request.

Conflicts of Interest

The authors declare no conflict of interest.

References

[1] H. P. Xie, F. Gao, and Y. Ju, "Research and development of rock mechanics in deep ground engineering," *Chinese Journal of Rock Mechanics and Engineering*, vol. 34, no. 11, pp. 2161–2178, 2015.

[2] H. P. Xie, "Research framework and anticipated results of deep rock mechanics and mining theory," *Advanced Engineering*, vol. 39, no. 2, p. 3, 2017.

[3] M. C. He, H. P. Xie, S. P. Peng, and Y. D. Jiang, "Study on rock mechanics in deep mining engineering," *Chinese Journal of Rock Mechanics and Engineering*, vol. 24, no. 16, pp. 2803–2813, 2005.

[4] B. N. Hu, "Backfill mining technology and development tendency in China coal mine," *Coal Science and Technology*, vol. 40, no. 11, p. 2, 2012.

[5] N. Sivakugan, R. Veenstra, and N. Naguleswaran, "Underground mine backfilling in Australia using paste fills and hydraulic fills," *International Journal of Geosynthetics and Ground Engineering*, vol. 1, no. 2, p. 18, 2015.

[6] H. A. Jati, N. Monei, G. Barakos, M. Tost, and M. Hitch, "Coal slurry pipelines: a coal transportation method in Kalimantan, Indonesia," *International Journal of Mining, Reclamation and Environment*, vol. 35, no. 9, pp. 638–655, 2021.

[7] Z. Q. Hu, W. Xiao, P. J. Wang, and Y. L. Zhao, "Concurrent mining and reclamation for underground coal mining," *Journal of China Coal Society*, vol. 38, no. 2, p. 301, 2013.

[8] D. J. Béket, L. Li, and P. Yang, "Experimental study of uniaxial compressive strength (UCS) distribution of hydraulic backfill associated with segregation," *Minerals*, vol. 9, no. 3, p. 147, 2019.

[9] H. Xu, D. B. Apel, J. Wang, C. Wei, and Y. Pourrahimian, "Investigation of backfilling step effects on stope stability," *Mining*, vol. 1, no. 2, pp. 155–166, 2021.

[10] D. F. Wang, G. Barakos, Z. Cheng, H. Mischo, and J. Zhao, "Numerical simulation of pressure profile of mining backfill fly-ash slurry in an L-shaped pipe using a validated Herschel-Bulkley model," *Journal of Sustainable Cement-Based Materials*, 2022.

[11] A. Lesmana and M. Hitch, "Heavy media coal hydro-transport in Malinau, Indonesia: a process study," *Journal of Mining and Mineral Engineering*, vol. 3, no. 1, pp. 1–15, 2011.

[12] H. A. Jati, N. Monei, G. Barakos, M. Tost, and M. Hitch, "Coal slurry pipelines: a coal transportation method in Kalimantan Indonesia," *Journal of Mining, Reclamation and Environment*, vol. 35, no. 9, pp. 638–655, 2021.

[13] S. Chandel, V. Seshadri, and S. N. Singh, "Effect of additive on pressure drop and rheological characteristics of fly ash slurry at high concentration," *Particulate Science and Technology*, vol. 27, no. 3, pp. 271–284, 2009.

[14] Q. Zhang, Z. Jiang, S. Wang, Q. Chen, Y. Zhu, and X. Hw, "Pipeline resistance model for the filling slurry transportation

with high concentration and superfine total tailing," *Science & Technology Review*, vol. 32, no. 24, pp. 51–55, 2014.

[15] C. Qi, Q. Chen, A. Fourie, J. Zhao, and Q. Zhang, "Pressure drop in pipe flow of cemented paste backfill: experimental and modeling study," *Powder Technology*, vol. 333, no. 2018, pp. 9–18, 2018.

[16] L. Liu, Z. Fang, C. Qi, B. Zhang, L. Guo, and K. I. I. L. Song, "Numerical study on the pipe flow characteristics of the cemented paste backfill slurry considering hydration effects," *Powder Technology*, vol. 343, pp. 454–464, 2019.

[17] X. Chen, J. Zhou, Q. Chen, X. Shi, and Y. Gou, "CFD simulation of pipeline transport properties of mine tailings three-phase foam slurry backfill," *Minerals*, vol. 7, no. 8, p. 149, 2017.

[18] A. X. Wu, Y. Yang, H. Y. Cheng, S. M. Chen, and Y. Han, "Status and prospects of paste technology in China," *Chinese Journal of Engineering*, vol. 40, no. 5, 525 pages, 2018.

[19] J. Singh, S. Kumar, J. P. Singh, P. Kumar, and S. K. Mohapatra, "CFD modeling of erosion wear in pipe bend for the flow of bottom ash suspension," *Particulate Science and Technology*, vol. 37, no. 3, pp. 275–285, 2019.

[20] S. Lahiri and K. C. Ghanta, "Regime identification of slurry transport in pipelines: a novel modelling approach using ANN & differential evolution," *Chemical Industry and Chemical Engineering Quarterly*, vol. 16, no. 4, pp. 329–343, 2010.

[21] M. Swamy, D. N. Gonzalez, and A. Twerda, "Numerical modelling of the slurry flow in pipelines and prediction of flow regimes," *WIT Transactions on Engineering Sciences*, vol. 89, pp. 311–322, 2015.

[22] J. Zhang, F. Darihaki, and S. A. Shirazi, "A comprehensive CFD-based erosion prediction for sharp bend geometry with examination of grid effect," *Wear*, vol. 430-431, pp. 191–201, 2019.

[23] M. C. Nuno, B. B. Martins, M. Silvia, M. R. Helena, and I. C. Dídia, "Efficient computational fluid dynamics model for transient laminar flow modeling: pressure wave propagation and velocity profile changes," *Journal of Fluids Engineering*, vol. 140, no. 1, 2018.

[24] N. Ratkovich, W. Horn, F. P. Helmus et al., "Activated sludge rheology: a critical review on data collection and modelling," *Water Research*, vol. 47, no. 2, pp. 463–482, 2013.

[25] J. Singh, M. Rudman, H. M. Blackburn, A. Chryss, L. Pullum, and L. J. W. Graham, "The importance of rheology characterization in predicting turbulent pipe flow of generalized Newtonian fluids," *Journal of Non-Newtonian Fluid Mechanics*, vol. 232, pp. 11–21, 2016.

[26] V. Khandelwal, A. Dhiman, and L. Baranyi, "Laminar flow of non-Newtonian shear-thinning fluids in a T-channel," *Computers and Fluids*, vol. 108, pp. 79–91, 2015.

[27] B. Bharathan, M. McGuinness, S. Kuhar, M. Kermani, F. P. Hassani, and A. P. Sasmito, "Pressure loss and friction factor in non-Newtonian mine paste backfill: modelling, loop test and mine field data," *Powder Technology*, vol. 344, no. 15, pp. 443–453, 2019.

[28] N. Gharib, B. Bharathan, L. Amiri, M. McGuinness, F. P. Hassani, and A. P. Sasmito, "Flow characteristics and wear prediction of Herschel-Bulkley non-Newtonian paste backfill in pipe elbows," *The Canadian Journal of Chemical Engineering*, vol. 95, no. 6, pp. 1181–1191, 2017.

[29] D. Mehta, A. Krishnan, T. Radhakrishnan, J. B. van Lier, and F. H. Clemens, "Assessment of numerical methods for estimating the wall shear stress in turbulent Herschel-Bulkley slurries in circular pipes," *Journal of Hydraulic Research*, vol. 59, no. 2, pp. 196–213, 2021.

[30] Y. Huang, W. Zheng, D. Zhang, and Y. Xi, "A modified Herschel–Bulkley model for rheological properties with temperature response characteristics of polysulfonated drilling fluid," *Energy Sources, Part A: Recovery, Utilization, and Environmental Effects*, vol. 42, no. 12, pp. 1464–1475, 2020.

[31] H. Taibi and F. Messelmi, "Effect of yield stress on the behavior of rigid zones during the laminar flow of Herschel-Bulkley fluid," *Alexandria Engineering Journal*, vol. 57, no. 2, pp. 1109–1115, 2018.

[32] L. Sun, G. Q. Zhao, and G. T. Yeh, "Automatic triangular and triangular-prism mesh generation for overland and subsurface water flow simulations," *Physics of Fluids*, vol. 32, no. 5, article 056602, 2020.

[33] L. Sun, G.-T. Yeh, F. P. Lin, and G. Zhao, "Automatic quadrilateral mesh generation and quality improvement techniques for an improved combination method," *Computational Geosciences*, vol. 19, no. 2, pp. 371–388, 2015.

[34] T. D. Blacker and M. B. Stephenson, "Paving: a new approach to automated quadrilateral mesh generation," *International Journal for Numerical Methods in Engineering*, vol. 32, no. 4, pp. 811–847, 1991.

[35] M. Yerry and M. Shephard, "A modified quadtree approach to finite element mesh generation," *IEEE Computer Graphics and Applications*, vol. 3, no. 1, pp. 39–46, 1983.

[36] L. Sun, G. Zhao, and X. Ma, "Quality improvement methods for hexahedral element meshes adaptively generated using grid-based algorithm," *International Journal for Numerical Methods in Engineering*, vol. 89, no. 6, pp. 726–761, 2012.

[37] N. Kumar, G. M. Kumar, and D. R. Kaushal, "Experimental investigations and CFD modeling for flow of highly concentrated iron ore slurry through horizontal pipeline," *Particulate Science and Technology*, vol. 37, no. 2, pp. 232–250, 2019.

[38] F. T. Pinho and J. H. Whitelaw, "Flow of non-Newtonian fluids in a pipe," *Journal of Non-Newtonian Fluid Mechanics*, vol. 34, no. 2, pp. 129–144, 1990.

[39] D. Picchi, A. Ullmann, and N. Brauner, "Modeling of core-annular and plug flows of Newtonian/non-Newtonian shear-thinning fluids in pipes and capillary tubes," *Journal of Multiphase Flow*, vol. 103, no. 1, pp. 43–60, 2018.

[40] I. M. Yusri, A. P. P. Abdul Majeed, R. Mamat, M. F. Ghazali, O. I. Awad, and W. H. Azmi, "A review on the application of response surface method and artificial neural network in engine performance and exhaust emissions characteristics in alternative fuel," *Renewable and Sustainable Energy Reviews*, vol. 90, pp. 665–686, 2018.

[41] K. S. Kazeem, O. A. Akeem, and D. A. Mohammed, "Application of response surface methodology for the modelling and optimization of sand minimum transport condition in pipeline multiphase flow," *Petroleum and Coal*, vol. 60, no. 2, pp. 339–348, 2018.